HHS Public Access

Author manuscript

Ann Neurol. Author manuscript; available in PMC 2019 February 06.

Published in final edited form as:

Ann Neurol. 2018 February ; 83(2): 248–257. doi:10.1002/ana.25142.

[^{18}F]AV-1451 clustering of entorhinal and cortical uptake in Alzheimer's disease

Jennifer L. Whitwell, PhD[1], **Jonathan Graff-Radford, MD**[2], **Nirubol Tosakulwong, BS**[3], **Stephen D. Weigand, MS**[3], **Mary Machulda, PhD**[4], **Matthew L. Senjem, MS**[1,5], **Christopher G. Schwarz, PhD**[1], **Anthony J. Spychalla, BS**[1], **David T. Jones, MD**[2], **Daniel A. Drubach, MD**[2], **David S. Knopman, MD**[2], **Bradley F. Boeve, MD**[2], **Nilüfer Ertekin-Taner, MD, PhD**[6,7], **Ronald C. Petersen, MD, PhD**[2], **Val J. Lowe, MD**[1], **Clifford R. Jack Jr., MD**[1], and **Keith A. Josephs, MD, MST, MSc**[2]

[1]Department of Radiology, Mayo Clinic, Rochester, MN

[2]Department of Neurology, Mayo Clinic, Rochester, MN

[3]Department of Health Sciences Research, Mayo Clinic, Rochester, MN

[4]Department of Psychology and Psychiatry, Mayo Clinic, Rochester, MN

[5]Department of Information Technology, Mayo Clinic, Rochester, MN

[6]Department of Neurology, Mayo Clinic, Jacksonville, FL

[7]Department of Neuroscience, Mayo Clinic, Jacksonville, FL

Abstract

Objective—To use a cluster analysis of [^{18}F]AV-1451 tau-PET data to determine how subjects with Alzheimer's disease vary in the relative involvement of the entorhinal cortex and neocortex, and determine whether relative involvement of these two regions can help explain variability in age and clinical phenotype in Alzheimer's disease.

METHODS—We calculated [^{18}F]AV-1451 uptake in entorhinal cortex and neocortex in 62 amyloid-positive Alzheimer's disease patients (39 typical and 23 atypical presentation). Tau-PET values were normalized to the cerebellum to create SUVRs. Tau-PET SUVRs were log-transformed and clustered blinded to clinical information into three groups using K-median cluster analysis. Demographics, clinical phenotype, cognitive performance, and apolipoprotein e4 frequency were compared across clusters.

RESULTS—The cluster analysis identified a cluster with low entorhinal and cortical uptake (E^{Lo}/C^{Lo}), one with low entorhinal but high cortical uptake (E^{Lo}/C^{Hi}), and one with high cortical

Corresponding author: Jennifer L. Whitwell, PhD, Associate Professor of Radiology, Mayo Clinic, 200 1st St SW, Rochester, MN 55905, Tel: 507-284-5576, Fax: 507-284-9778, Whitwell.jennifer@mayo.edu.

AUTHOR CONTRIBUTIONS

Conception and design of the study: JLW, NT, SDW, KAJ

Acquisition and analysis of data: JLW, JGR, NT, SDW, MMM, MLS, CGS, AJS, DTJ, DAD, DSK, BFB, NET, RCP, VJL, CRJ, KAJ

Drafting the manuscript: JLW, KAJ

POTENTIAL CONFLICTS OF INTEREST

The authors do not have any conflicts of interest relevant to this manuscript

and entorhinal uptake (E^{Hi}/C^{Hi}). Clinical phenotype differed across clusters, with typical AD most commonly observed in the E^{Lo}/C^{Lo} and E^{Hi}/C^{Hi} clusters, and atypical AD most commonly observed in the E^{Lo}/C^{Hi} cluster. The E^{Lo}/C^{Lo} cluster had an older age at PET and onset than the other clusters. The apolipoprotein e4 frequency was lower in the E^{Lo}/C^{Hi} cluster. The E^{Hi}/C^{Hi} cluster had the worst memory impairment, while the E^{Lo}/C^{Hi} cluster had the worst impairment in non-memory domains.

INTERPRETATION—This study demonstrates considerable variability in [^{18}F]AV-1451 tau-PET uptake in AD, but shows that a straight-forward clustering based on entorhinal and cortical uptake maps well onto age and clinical presentation in AD.

INTRODUCTION

Alzheimer's disease (AD) is a heterogeneous neurodegenerative disease characterized by neuritic beta-amyloid plaques and tau neurofibrillary tangles[1–3] which can present with different clinical syndromes and affects people ranging from the fifth to the tenth decade of life. The most common clinical presentation of AD is dominated by episodic memory loss. These patients are diagnosed with typical Alzheimer's dementia[4]. However, AD patients can present with atypical clinical syndromes where loss of episodic memory is not the earliest or most prominent feature[5, 6]. Atypical AD subjects can instead show the most prominent impairments in language, visuospatial/perceptual function, or executive function/behavior[6]. The typical clinical presentation of AD can occur both in young-onset (under age 65 years) and late-onset (over age 65 years) patients, while the atypical clinical presentations tend to most commonly occur in young-onset patients.

Magnetic Resonance Imaging studies performed at the group-level typically find that the different variants of AD are associated with different degrees of atrophy of the cortex and medial temporal lobe. Young-onset typical AD patients have been shown to have a greater degree of cortical atrophy compared to late-onset AD patients which show patterns of atrophy restricted to the medial temporal lobe[7–10]. Cortical atrophy is also typically observed in atypical AD patients, with these patients showing a relative sparing of medial temporal lobe structures[11–13]. Evidence from studies with neuroimaging and pathology suggest that these differing patterns relate to the distribution of underlying tau pathology in the brain[5, 14–16], and, therefore, that tau topography is the key driver of both atrophy and clinical presentation in AD.

Positron emission tomography (PET) ligands, such as [^{18}F]AV-1451[17], are now available that allow the detection of tau in the brain during life, and hence allow the direct assessment of how tau topography relates to clinical presentation in AD. The [^{18}F]AV-1451 ligand has been shown to bind strongly to AD tau in autoradiographic studies[18–20] and shows striking uptake in AD patients[21–24]. Recent group-level studies with [^{18}F]AV-1451 have shown that the atypical variants of AD show striking cortical uptake of tau[25, 26]. Cortical uptake has also been observed in both young-onset and old-onset AD, although cortical uptake appears greater in young-onset AD[27, 28]. The aim of our study was to take an individual patient-level approach and utilize a straight forward cluster analysis of regional [^{18}F]AV-1451 uptake values blinded to clinical diagnosis, to determine how well tau topography matches with

clinical presentation (typical versus atypical) and age in AD. Given previous neuroimaging and autopsy studies, we based the cluster analysis on tau uptake in the medial temporal lobe and neocortex with the hypothesis that the relative involvement of these two regions will explain much of the variability in clinical presentation in AD.

METHODS

Subjects

We identified all patients with a clinical diagnosis of typical or atypical AD that had evidence of beta-amyloid deposition on Pittsburgh Compound B (PiB) PET and had undergone [^{18}F]AV-1451 tau-PET at Mayo Clinic, Rochester, MN. Sixty-two patients were identified, of which 39 had early and significant memory impairment and were diagnosed with typical AD[4]. The remaining 23 patients were diagnosed with atypical AD[6], of which 9 were diagnosed with posterior cortical atrophy[29], 7 were diagnosed with logopenic aphasia[13], and 7 were diagnosed with behavioral/dysexecutive AD[30]. None of the subjects in the study met criteria for mild cognitive impairment[31]. These patients had been recruited as part of an NIH-funded grant studying atypical AD (PI Whitwell) or as part of the Mayo Clinic Alzheimer's Disease Research Center (PI Petersen). All patients, regardless of recruitment mechanism, underwent a detailed neurological examination by a behavioral neurologist and diagnoses were rendered based on established clinical criteria. Clinical and neuropsychological tests that were available for analysis across both cohorts included the Clinical Dementia Rating (CDR) scale to measure functional impairment, Trail Making Tests A and B to measure processing speed and executive function, letter (F) and animal fluency to assess executive control and lexical access, Auditory Verbal Learning Test (AVLT) to assess memory, and the Rey-Osterrieth (Rey-O) Complex Figure Test – Copy Trial to assess visuospatial function. Disease duration was calculated as time from the initial symptom reported by the patient and carer to the time of PET scan. Apolioprotein E (APOE) genotyping was also performed. The study was approved by the Mayo IRB. All subjects consented to research.

Image acquisition

Tau-PET imaging was performed using the [^{18}F]AV-1451 ligand and amyloid-PET imaging was performed using PiB-PET. All PET scans were acquired using a PET/CT scanner (GE Healthcare, Milwaukee, Wisconsin) operating in 3D mode. For tau-PET, an intravenous bolus injection of approximately 370MBq (range 333-407 MBq) of [^{18}F]AV-1451 was administered, followed by a 20 minute PET acquisition performed from 80 to 100 minutes after injection. For PiB-PET, participants were injected with PiB of approximately 628 MBq (range, 385-723 MBq) and a 20 minute PET acquisition was performed from 40 to 60 minutes after injection. Both 20-minute late-uptake PET scans consisted of four, five minute dynamic frames following a low dose CT image obtained for attenuation correction. Vendor supplied corrections for attenuation, scatter, and randoms corrections were applied. PET sinograms were iteratively reconstructed into a 256mm FOV. The pixel size was 1.0mm and the slice thickness 3.3 mm. The four individual frames of each dynamic series were averaged to create a 20-minute mean summed image that was used for analysis. All subjects had a 3T MPRAGE sequence performed on the same day as the tau-PET, as previously

described[32]. The PiB-PET scans were used as part of the inclusion criteria of the study to ensure all subjects had beta-amyloid deposition consistent with the presence of AD pathology. A global PiB standard uptake value ratio (SUVR) was generated as previously described[33] using the cerebellar crus grey matter as a reference region, and a cut-point of 1.42[33] was used to define the presence of beta-amyloid deposition.

Tau-PET analysis

All image processing steps were performed using SPM12 (www.fil.ion.ucl.ac.uk/SPM). [18F]AV-1451 images were registered to the subjects MPRAGE using 6-degree-of-freedom rigid body registration. Normalization parameters were computed between each MPRAGE and the Mayo Clinic Adult Lifespan Template (MCALT) (https://www.nitrc.org/projects/mcalt/) using ANTs[34]. With these parameters, the MCALT atlases were propagated to native MPRAGE space and used to calculate regional [^{18}F]AV-1451 uptake in the grey and white matter. Tissue probabilities were determined by segmenting each MPRAGE using Unified Segmentation[35] in SPM12 with the MCALT tissue priors. Tissue-type masks were created by using these probabilistic segmentations of each tissue class to determine which class had the maximum probability. These segmentations were used to create masks of grey + white matter to refine the borders of atlas regions. Median [^{18}F]AV-1451 uptake was calculated for the entorhinal cortex (ERC) and for a neocortical region-of-interest (ROI). We selected the entorhinal cortex to represent the medial temporal lobe, instead of the hippocampus, because hippocampal [^{18}F]AV-1451 measurements can be confounded by off-target uptake in the choroid plexus[18, 36]. The neocortical ROI was generated by calculating median uptake across 17 cortical regions of the brain, including lateral temporal gyri and medial and lateral parietal, occipital and frontal regions. Left and right hemisphere structures were combined for the entorhinal cortex and the neocortical ROI. Median [^{18}F]AV-1451 uptake in each ROI was divided by median uptake in cerebellar crus grey matter to create SUVRs. Regional grey matter volumes for the ERC and neocortical ROIs were summed from voxel-wise grey matter probabilities within the grey and white matter masks, within each atlas ROI. Total intracranial volumes were summed from the SPM12 grey, white and CSF segmentations[37], and used to correct regional volumes for head size.

A voxel-level analysis was also performed to examine global patterns of uptake in each cluster compared to a cohort of 62 age and gender matched controls (median [IQR] age at PET=68 [59, 75], No. female=33 (53%)) that were selected from the Mayo Clinic Study of Aging[38]. The MCALT atlases in MPRAGE space were used to divide all voxels in the MPRAGE-space [^{18}F]AV-1451 images by the median uptake in the cerebellar crus grey matter to create SUVR images. These SUVR images were normalized to the MCALT using SPM12 normalization parameters from the MPGRAGE and smoothed at 6 mm full-width at half maximum. Voxel-level comparisons were performed using two-sided T-tests in SPM12, with results assessed at $p<0.001$ after correction for multiple comparisons using the family wise error correction. Age and gender were included in the analysis as covariates.

Statistics

We used the k-medians algorithm to cluster log-transformed entorhinal cortex and neocortical tau PET SUVR. When performing k-median clustering, we need to specify the

number of clusters (k) beforehand. We used two methods to help us choose an appropriate number of clusters. First, we used the "elbow method" which utilizes the sum of within-cluster distances. We performed k-median clustering on the dataset from 2 clusters to 10 clusters and for each number of clusters the sum of within-cluster distances was calculated. We then plotted the sum of within-cluster distances against the number of clusters (elbow plot). The sum of within-cluster distances will decrease with increasing number of clusters. The general idea is to try to minimize the sum of within-cluster distances, while choosing the smallest possible cluster size where adding one more cluster will offer little marginal improvements in the sum of within-cluster distances. Second, we assessed the stability, or reproducibility, of clusters by performing bootstrap resampling with 100 replicates[39]. For each replicate two random samples were drawn with replacement and k-medians clustering is performed on each sample. The original subjects were then classified based on each of these replicate clusters and the agreement, or concordance, was assessed via the adjusted Rand index (ARI). The ARI summarizes the fraction of all pairs of subjects for which the two replicate clusterings agree after accounting for chance agreement[40, 41]. Higher values of ARI indicate stronger agreement. We summarize the separation of the resulting clustering via a scatter plot of the two principal components and overlaying ellipses drawn to include all points in each cluster.

Demographics, clinical and cognitive variables were compared between the three clusters using Fisher's exact tests for categorical variables or nonparametric Kruskal-Wallis tests followed by Wilcoxon rank sum tests for continuous variables. $P < 0.05$ was considered statistically significant. Analyses were performed with R statistical software version 3.1.3 (R Foundation for Statistical Computing, Vienna, Austria) and the "flexclust" package.

RESULTS

Cluster results

Based on the elbow method and the adjusted Rand index statistics we determined that three clusters were appropriate for this data set. The elbow method showed that three clusters appreciably reduced the sum of within cluster distances compared to just two clusters, with four clusters showing less additional reduction (Fig 1A). The ARI analysis showed that cluster stability was similar for both three and four clusters (Fig 1B).

A scatter-plot depicting the three clusters is shown in Fig 2A. One cluster (n=21) was characterized by relatively low tau uptake compared to the rest of the cohort in both the ERC and cortex (E^{Lo}/C^{Lo}) (**red**, Fig 2A). The rest of the patients showed relatively high cortical tau uptake, with one cluster (n=21) characterized by relatively low ERC and high cortical uptake compared to the rest of the cohort (E^{Lo}/C^{Hi}) (**green**, Fig 2A) and one cluster (n=20) characterized by high tau uptake in both the ERC and cortex (E^{Hi}/C^{Hi}) (**blue**, Fig 2A). Figure 2B shows the data in terms of its two (uncorrelated) principal components with ellipses representing the clusters. The plot showed excellent separation between the E^{Lo}/C^{Lo} cluster and the other two clusters, with the most overlap observed between the E^{Lo}/C^{Hi} and E^{Hi}/C^{Hi} clusters. The similarity between the relationship between ERC and cortical tau and the principal component analysis also suggests that the ERC and cortical SUVRs are

generally independent tau metrics; the first principal component is primarily cortical tau, and the second primarily ERC tau.

The group-level ERC SUVRs had a median (IQR) of 1.95 (1.85, 2.03) in the E^{Hi}/C^{Hi} cluster compared to medians of 1.60 (1.48, 1.78) in the E^{Lo}/C^{Lo} cluster and 1.55 (1.48, 1.63) in the E^{Lo}/C^{Hi} cluster (Table 1). The E^{Lo}/C^{Lo} cluster had a neocortical SUVR of 1.41 (1.32, 1.48) compared to 1.88 (1.78, 2.19) in the E^{Lo}/C^{Hi} and 2.12 (2.04, 2.49) in the E^{Hi}/C^{Hi} clusters. The ratio of ERC-to-cortical SUVR was higher in the E^{Lo}/C^{Lo} cluster (1.13 [1.02, 1.23]) compared to the E^{Lo}/C^{Hi} (0.79 [0.68, 0.91]) and E^{Hi}/C^{Hi} (0.87 [0.81, 1.00]) clusters. The voxel-level patterns of tau-PET uptake in each cluster compared to controls are shown in Fig 3. The E^{Lo}/C^{Lo} cluster showed focal uptake bilaterally in the ERC, parahippocampal gyrus, amygdala, hippocampus, fusiform gyrus, inferior and middle temporal gyri and posterior cingulate compared to controls. The E^{Lo}/C^{Hi} and E^{Hi}/C^{Hi} clusters both showed tau-PET uptake throughout the temporoparietal lobes, posterior cingulate, precuneus, medial and lateral frontal lobes, occipital lobe, ERC, parahippocampal gyrus, amygdala and fusiform gyrus compared to controls, although the degree of uptake was generally greater in the E^{Hi}/C^{Hi} cluster and the hippocampus was also involved. Both the E^{Lo}/C^{Hi} and E^{Hi}/C^{Hi} clusters showed greater cortical uptake than the E^{Lo}/C^{Lo} cluster, and the E^{Hi}/C^{Hi} cluster also showed greater uptake in the ERC, parahippocampal gyrus and amygdala than the E^{Lo}/C^{Lo} cluster. The E^{Hi}/C^{Hi} cluster showed greater uptake in amygdala, ERC, hippocampus, inferior and middle temporal lobes and posterior cingulate than the E^{Lo}/C^{Hi} cluster.

Clinical correlates of the cluster analysis

The distribution of typical versus atypical clinical phenotype differed across clusters ($p<0.001$) (Table 1). The majority of subjects in both the E^{Lo}/C^{Lo} (81%) and E^{Hi}/C^{Hi} (80%) clusters had a clinical diagnosis of typical AD, whereas the majority of the subjects in the E^{Lo}/C^{Hi} cluster had a diagnosis of atypical AD (Fig 2A). The distribution of the specific atypical clinical diagnoses did not differ across the three clusters, with most of the dysexecutive (71%), logopenic (43%) and posterior cortical atrophy (78%) cases clustered into the E^{Lo}/C^{Hi} cluster. Significant differences were observed across clusters in age at scan and age at onset, with the E^{Lo}/C^{Hi} and E^{Hi}/C^{Hi} clusters at least a decade younger on average compared to the E^{Lo}/C^{Lo} cluster (Table 1). Fig 4 shows that the majority of subjects in the E^{Lo}/C^{Lo} cluster were over the age of 65 at the time of PET, except for one atypical AD subject. In contrast, the majority of subjects in the E^{Hi}/C^{Hi} cluster were under age 65. The subjects in the E^{Lo}/C^{Hi} cluster consisted of subjects under and over age 65.

In addition, disease duration was longer in the E^{Lo}/C^{Lo} cluster compared to the E^{Lo}/C^{Hi} cluster, and the E^{Lo}/C^{Hi} and E^{Hi}/C^{Hi} clusters both showed a lower global PiB ratio than the E^{Lo}/C^{Lo} cluster (Table 1). The proportion of APOE e4 carriers was lower in the E^{Lo}/C^{Hi} cluster compared to the E^{Lo}/C^{Lo} cluster. There were also some differences across clusters in cognitive performance, with the E^{Hi}/C^{Hi} group showing the worst performance on the AVLT Delayed % recall, and the E^{Lo}/C^{Hi} cluster showing worst performance on the Trail Making Test A and Rey-O.

DISCUSSION

This study demonstrates that the severity of ERC and neocortical [^{18}F]AV-1451 tau-PET uptake varies considerably across the AD spectrum, and that the degree of uptake in these two regions maps well onto clinical presentation and age in AD.

The cluster analysis utilized in this study was blinded to diagnosis and showed that patients best clustered into three groups when ERC and cortical tau uptake was considered. Most notably, the E^{Lo}/C^{Lo} cluster consisted of 35% of the cohort with subjects showing very little cortical uptake, but also relatively low levels of ERC uptake. At the group-level tau uptake in the ERC was greater than observed in controls, although the degree of ERC uptake was relatively low compared to the rest of our cohort. Elevated uptake was also observed in these subjects in other temporal regions, including the hippocampus, and in the posterior cingulate which is functionally and structurally connected to the hippocampus[42]. The patients in the other two clusters all showed cortical uptake, particularly involving temporoparietal cortices, but also frontal and occipital lobes demonstrating widespread cortical tau uptake in these subjects and suggesting they may have high Braak stage[1]. These patterns are similar to previous studies that have reported group-level patterns of [^{18}F]AV-1451 uptake in Alzheimer's dementia[22–24], that also show quite widespread patterns of cortical uptake. Of these cortical clusters, the E^{Hi}/C^{Hi} cluster showed a greater degree of uptake in the ERC and cortical ROI, compared to the E^{Lo}/C^{Hi} cluster.

Regional heterogeneity in neurofibrillary tangle deposition in AD has been previously recognized at autopsy, with subdivision of cases based on relative involvement of hippocampus and cortex[43]. A limbic-predominant variant was described that shows high neurofibrillary tangle counts in the hippocampus but a relative sparing of cortex, and a hippocampal sparing variant was described showing high neurofibrillary tangle counts in the cortex but relative sparing of the hippocampus[43]. The E^{Lo}/C^{Lo} cluster would most closely fit with the limbic-predominant variant, although the degree of tau uptake in the ERC was still relatively low in these subjects. It was somewhat surprising that we did not identify a tau-PET variant with low cortical uptake and high ERC uptake. It appears, instead, as though high ERC uptake is usually observed in the context of high cortical uptake. The E^{Lo}/C^{Hi} cluster would be most akin to the hippocampal sparing variant; in fact this was the only cluster that did not show evidence for elevated uptake in the hippocampus. Surprisingly, the ERC-cortex ratio did not differ between the E^{Lo}/C^{Hi} and E^{Hi}/C^{Hi} clusters, suggesting these clusters were not separated based on the relative involvement of these regions, but the severity of involvement of these regions. Discrepancies with autopsy classification may, however, be expected given that we are assessing tau distribution earlier in the disease course rather than at death. It is possible, for example, that the E^{Lo}/C^{Lo} cluster could develop high ERC uptake by death.

Age and clinical presentation mapped well onto our three [^{18}F]AV-1451-based clusters, supporting the validity and significance of the cluster analysis. The E^{Lo}/C^{Lo} cluster was significantly older at scan than the other clusters, consisting almost exclusively of patients over the age of 65 years. These findings concur with one previous [^{18}F]AV-1451 study that similarly showed that late onset AD patients had less tau uptake in cortical regions than

young onset AD[27]. The subjects in the E^{Lo}/C^{Lo} cluster showed some mild [^{18}F]AV-1451 uptake in the ERC and other medial temporal regions, suggesting they may have a low Braak stage[1] and likely explaining why the majority of subjects in this cluster presented with a typical AD clinical presentation dominated by memory impairment. The E^{Hi}/C^{Hi} cluster was also strongly associated with a typical AD presentation, but the subjects had a significantly younger age. It therefore appears as though young subjects with typical AD are particularly likely to show striking uptake in both the ERC and cortex. Memory impairment was also worse in these subjects compared to the E^{Lo}/C^{Lo} cluster, reflecting the greater tau burden of the ERC. Importantly, disease duration did not differ between the E^{Lo}/C^{Lo} and E^{Hi}/C^{Hi} clusters, and so the E^{Hi}/C^{Hi} cluster does not seem to be a more advanced version of the E^{Lo}/C^{Lo} cluster. The fact that tau uptake in the ERC was higher in the young subjects in the E^{Hi}/C^{Hi} cluster compared to the older subjects in the E^{Lo}/C^{Lo} cluster, conflicts somewhat with some previous MRI studies that have found greater medial temporal atrophy in old compared to young-onset AD[7, 10]. The reason for this discordance is unclear but our finding of high ERC uptake in young AD makes sense given the fact that these subjects still had dominant memory impairment despite the high degree of cortical involvement. Volumes of the ERC and cortex somewhat reflected the tau findings (i.e. more atrophy relating to greater tau uptake); although the volumes did not differ across clusters suggesting that atrophy may be less sensitive to detect these clusters.

The E^{Lo}/C^{Hi} cluster was also associated with young age; again supporting an association between age and cortical tau. However, the E^{Lo}/C^{Hi} cluster was more likely to be associated with an atypical clinical presentation of AD compared to either of the other clusters. The E^{Lo}/C^{Hi} cluster also showed poorer performance on tests of cognitive speed, executive function and visuospatial function compared to the other clusters. This cluster showed the lowest ERC-cortex ratio, reflecting relatively less involvement of the ERC compared to cortex. Hence, we could hypothesize that the presence of atypical syndromes in this cluster is because the symptomatology coming from the cortex dominates over memory impairment coming from the medial temporal lobe. The reason that patients in the E^{Lo}/C^{Hi} cluster also showed lower cortical uptake than patients in the E^{Hi}/C^{Hi} cluster is unclear, but suggests that atypical AD subjects are different from young-onset typical AD subjects in the degree of both cortical and ERC tau uptake. However, asymmetry is often a feature of atypical AD[12, 13, 44], and hence it is also possible that asymmetry in the patterns of cortical tau may have reduced the total cortical SUVR in this cluster which is averaged across both hemispheres.

We found a lower frequency of APOE e4 carriers in the E^{Lo}/C^{Hi} cluster, with only 48% of e4 carriers. Several studies report that APOE e4 frequency is lower in atypical clinical presentations compared to typical AD[23, 45–47]. Our results fit with these findings but extend them to show that a lower APOE e4 frequency is particularly associated with high tau deposition in the cortex but a relative sparing of the ERC. Conversely, higher APOE e4 frequencies were observed in the two clusters strongly associated with typical AD regardless of the pattern of tau deposition or average age of the cluster. Given the similarity in ERC uptake in the E^{Lo}/C^{Lo} and E^{Lo}/C^{Hi} clusters, our data does not support the notion that APOE e4 predisposes to medial temporal pathology[48]. We also observed a difference in global PiB

SUVR across our groups, with higher values showing greater beta-amyloid deposition, in the E^{Lo}/C^{Lo} cluster, possibly reflecting the older age of this cluster[49].

A strength of our study is the large number of subjects and that our cohort represented both typical and atypical variants of AD. It should be noted, however, that we had a large proportion of young subjects in our cohort, and hence the expected proportion of subjects in each cluster may not generalize to all settings. Some potential limitations of the study include possible contributions of measurement noise, which could particularly affect measurements in a small structure like the ERC. Quantification of other structures could also be influenced by signal in the white matter and edge effects from the ventricles, for example the posterior cingulate which showed tau uptake in all three clusters. A potential issue with SUVR quantification is contamination of the normalization area from off-target binding and adjacent cortical signal. The crus region was selected to provide cerebellar grey matter in relative isolation from CSF spaces and to avoid adjacency to potential bleed-in from occipital, parahippocampal, and fusiform tau-pathology[28]. It has been shown that the tracer is not at an entirely stable state during late-uptake scans, but SUVR appears to model tangles very well even though its sensitivity to blood flow is uncertain[50]. Future autopsy correlation will be needed for further confirmation of the robustness of SUVR calculations.

In summary, this study demonstrates considerable variability in [^{18}F]AV-1451 tau-PET uptake in AD. The findings suggest that considering uptake in the ERC and cortex will help explain some of clinical heterogeneity observed in AD. It will be crucially important for future tau-PET studies in AD to consider this variability and account for a subject's specific tau-PET profile. Tau-PET provides the ideal opportunity to generate disease biomarkers for use in therapeutic trials in AD but optimum biomarkers will almost certainly differ for the three clusters of subjects identified in this study. Stratification of subjects into one of these three groups using the degree of ERC and cortical tau uptake could be an important strategy in this regard to help appropriately target biomarkers and interpret therapeutic efficacy.

Acknowledgments

This study was funded by the National Institutes of Health (R01-AG50603, R21-NS94684, P50 AG16574, U01 AG006786, R01 AG11378, R01 AG041851, RF1 AG051504, U01 AG046139, and R01 NS080820). We would like to acknowledge AVID Radiopharmaceuticals for provision of AV-1451 precursor, chemistry production advice and oversight, and FDA regulatory cross-filing permission and documentation needed for this work.

References

1. Braak H, Braak E. Neuropathological stageing of Alzheimer-related changes. Acta neuropathologica. 1991; 82(4):239–59. [PubMed: 1759558]
2. Hyman BT, Phelps CH, Beach TG, et al. National Institute on Aging-Alzheimer's Association guidelines for the neuropathologic assessment of Alzheimer's disease. Alzheimers Dement. 2012 Jan; 8(1):1–13. [PubMed: 22265587]
3. Montine TJ, Phelps CH, Beach TG, et al. National Institute on Aging-Alzheimer's Association guidelines for the neuropathologic assessment of Alzheimer's disease: a practical approach. Acta neuropathologica. 2012 Jan; 123(1):1–11. [PubMed: 22101365]
4. McKhann GM, Knopman DS, Chertkow H, et al. The diagnosis of dementia due to Alzheimer's disease: recommendations from the National Institute on Aging-Alzheimer's Association workgroups on diagnostic guidelines for Alzheimer's disease. Alzheimers Dement. 2011 May; 7(3): 263–9. [PubMed: 21514250]

5. Whitwell JL, Dickson DW, Murray ME, et al. Neuroimaging correlates of pathologically defined subtypes of Alzheimer's disease: a case-control study. Lancet Neurol. 2012 Oct; 11(10):868–77. [PubMed: 22951070]
6. Dubois B, Feldman HH, Jacova C, et al. Advancing research diagnostic criteria for Alzheimer's disease: the IWG-2 criteria. Lancet Neurol. 2014 Jun; 13(6):614–29. [PubMed: 24849862]
7. Frisoni GB, Testa C, Sabattoli F, Beltramello A, Soininen H, Laakso MP. Structural correlates of early and late onset Alzheimer's disease: voxel based morphometric study. J Neurol Neurosurg Psychiatry. 2005 Jan; 76(1):112–4. [PubMed: 15608008]
8. Ishii K, Kawachi T, Sasaki H, et al. Voxel-based morphometric comparison between early- and late-onset mild Alzheimer's disease and assessment of diagnostic performance of z score images. AJNR Am J Neuroradiol. 2005 Feb; 26(2):333–40. [PubMed: 15709131]
9. Dickerson BC, Brickhouse M, McGinnis S, Wolk DA. Alzheimer's disease: The influence of age on clinical heterogeneity through the human brain connectome. Alzheimers Dement (Amst). 2017; 6:122–35. [PubMed: 28239637]
10. Moller C, Vrenken H, Jiskoot L, et al. Different patterns of gray matter atrophy in early- and late-onset Alzheimer's disease. Neurobiol Aging. 2013 Aug; 34(8):2014–22. [PubMed: 23561509]
11. Whitwell JL, Jack CR Jr, Kantarci K, et al. Imaging correlates of posterior cortical atrophy. Neurobiol Aging. 2007 Jul; 28(7):1051–61. [PubMed: 16797786]
12. Madhavan A, Whitwell JL, Weigand SD, et al. FDG PET and MRI in Logopenic Primary Progressive Aphasia versus Dementia of the Alzheimer's Type. PLoS One. 2013; 8(4):e62471. [PubMed: 23626825]
13. Gorno-Tempini ML, Hillis AE, Weintraub S, et al. Classification of primary progressive aphasia and its variants. Neurology. 2011 Mar; 76(11):15. 1006–14.
14. Josephs KA, Dickson DW, Murray ME, et al. Quantitative neurofibrillary tangle density and brain volumetric MRI analyses in Alzheimer's disease presenting as logopenic progressive aphasia. Brain Lang. 2013 Mar.:27.
15. Thaker AA, Weinberg BD, Dillon WP, et al. Entorhinal Cortex: Antemortem Cortical Thickness and Postmortem Neurofibrillary Tangles and Amyloid Pathology. AJNR Am J Neuroradiol. 2017 Mar.:09.
16. Whitwell JL, Josephs KA, Murray ME, et al. MRI correlates of neurofibrillary tangle pathology at autopsy: a voxel-based morphometry study. Neurology. 2008 Sep; 71(10):2. 743–9.
17. Xia CF, Arteaga J, Chen G, et al. [(18)F]T807, a novel tau positron emission tomography imaging agent for Alzheimer's disease. Alzheimers Dement. 2013 Nov; 9(6):666–76. [PubMed: 23411393]
18. Lowe VJ, Curran G, Fang P, et al. An autoradiographic evaluation of AV-1451 Tau PET in dementia. Acta Neuropathol Commun. 2016; 4(1):58. [PubMed: 27296779]
19. Marquie M, Normandin MD, Vanderburg CR, et al. Validating novel tau positron emission tomography tracer [F-18]-AV-1451 (T807) on postmortem brain tissue. Ann Neurol. 2015 Nov; 78(5):787–800. [PubMed: 26344059]
20. Sander K, Lashley T, Gami P, et al. Characterization of tau positron emission tomography tracer [F]AV-1451 binding to postmortem tissue in Alzheimer's disease, primary tauopathies, and other dementias. Alzheimers Dement. 2016 Feb.:15.
21. Chien DT, Bahri S, Szardenings AK, et al. Early clinical PET imaging results with the novel PHF-tau radioligand [F-18]-T807. J Alzheimers Dis. 2013 Jan; 34(2):1. 457–68. [PubMed: 23186990]
22. Johnson KA, Schultz A, Betensky RA, et al. Tau positron emission tomographic imaging in aging and early Alzheimer disease. Ann Neurol. 2016 Jan; 79(1):110–9. [PubMed: 26505746]
23. Schott JM, Crutch SJ, Carrasquillo MM, et al. Genetic risk factors for the posterior cortical atrophy variant of Alzheimer's disease. Alzheimers Dement. 2016 Aug; 12(8):862–71. [PubMed: 26993346]
24. Whitwell JL, Lowe VJ, Tosakulwong N, et al. [18 F]AV-1451 tau positron emission tomography in progressive supranuclear palsy. Mov Disord. 2017 Oct; 32(1):27. 124–33.
25. Ossenkoppele R, Schonhaut DR, Baker SL, et al. Tau, amyloid, and hypometabolism in a patient with posterior cortical atrophy. Ann Neurol. 2015 Feb; 77(2):338–42. [PubMed: 25448043]

26. Xia C, Makaretz SJ, Caso C, et al. Association of In Vivo [18F]AV-1451 Tau PET Imaging Results With Cortical Atrophy and Symptoms in Typical and Atypical Alzheimer Disease. JAMA Neurol. 2017 Apr; 74(4):01. 427–36.
27. Choi JY, Cho H, Ahn SJ, et al. "Off-Target" 18F-AV-1451 Binding in the Basal Ganglia Correlates with Age-Related Iron Accumulation. J Nucl Med. 2017 Aug.:03.
28. Lowe VJ, Wiste HJ, Senjem ML, et al. Widespread Brain Tau and its Association with Aging, Braak Stage, and Alzheimer's Dementia. Brain. 2017 IN PRESS.
29. Crutch SJ, Schott JM, Rabinovici GD, et al. Consensus classification of posterior cortical atrophy. Alzheimers Dement. 2017 Mar; 13(8):02. 870–84.
30. Ossenkoppele R, Pijnenburg YA, Perry DC, et al. The behavioural/dysexecutive variant of Alzheimer's disease: clinical, neuroimaging and pathological features. Brain. 2015 Sep; 138(Pt 9): 2732–49. [PubMed: 26141491]
31. Petersen RC. Mild cognitive impairment as a diagnostic entity. J Intern Med. 2004 Sep; 256(3): 183–94. [PubMed: 15324362]
32. Jack CR Jr, Lowe VJ, Senjem ML, et al. 11C PiB and structural MRI provide complementary information in imaging of Alzheimer's disease and amnestic mild cognitive impairment. Brain. 2008 Mar; 131(Pt 3):665–80. [PubMed: 18263627]
33. Jack CR Jr, Wiste HJ, Weigand SD, et al. Defining imaging biomarker cut points for brain aging and Alzheimer's disease. Alzheimers Dement. 2017 Mar; 13(3):205–16. [PubMed: 27697430]
34. Avants BB, Epstein CL, Grossman M, Gee JC. Symmetric diffeomorphic image registration with cross-correlation: evaluating automated labeling of elderly and neurodegenerative brain. Med Image Anal. 2008 Feb; 12(1):26–41. [PubMed: 17659998]
35. Ashburner J, Friston KJ. Unified segmentation. Neuroimage. 2005 Jul; 26(3):1. 839–51. [PubMed: 15862199]
36. Ikonomovic MD, Abrahamson EE, Price JC, Mathis CA, Klunk WE. [F-18]AV-1451 positron emission tomography retention in choroid plexus More than "off-target" binding. Ann Neurol. 2016 Aug; 80(2):307–8. [PubMed: 27314820]
37. Schwarz CG, Gunter JL, Wiste HJ, et al. A large-scale comparison of cortical thickness and volume methods for measuring Alzheimer's disease severity. Neuroimage Clin. 2016; 11:802–12. [PubMed: 28050342]
38. Roberts RO, Geda YE, Knopman DS, et al. The Mayo Clinic Study of Aging: design and sampling, participation, baseline measures and sample characteristics. Neuroepidemiology. 2008; 30(1):58–69. [PubMed: 18259084]
39. Dolnicar S, Leisch F. Evaluation of Structure and Reproducibility of Cluster Solutions Using the Bootstrap. Marketing Letters. 2010; 21(1):83–101.
40. Hubert L, Arabie P. Comparing partitions. J Classification. 1985; 2:193–218.
41. Rand WM. Objective criteria for the evaluation of clustering methods. J American Statistical Association. 1971; 66(336):846–50.
42. Greicius MD, Srivastava G, Reiss AL, Menon V. Default-mode network activity distinguishes Alzheimer's disease from healthy aging: evidence from functional MRI. Proc Natl Acad Sci U S A. 2004 Mar; 101(13):30. 4637–42.
43. Murray ME, Graff-Radford NR, Ross OA, Petersen RC, Duara R, Dickson DW. Neuropathologically defined subtypes of Alzheimer's disease with distinct clinical characteristics: a retrospective study. Lancet Neurol. 2011 Sep; 10(9):785–96. [PubMed: 21802369]
44. Whitwell JL, Graff-Radford J, Singh TD, et al. 18F-FDG PET in Posterior Cortical Atrophy and Dementia with Lewy Bodies. J Nucl Med. 2017 Apr; 58(4):632–8. [PubMed: 27688479]
45. Balasa M, Gelpi E, Antonell A, et al. Clinical features and APOE genotype of pathologically proven early-onset Alzheimer disease. Neurology. 2011 May; 76(20):17. 1720–5.
46. Carrasquillo MM, Khan Q, Murray ME, et al. Late-onset Alzheimer disease genetic variants in posterior cortical atrophy and posterior AD. Neurology. 2014 Apr; 82(16):22. 1455–62.
47. Josephs KA, Duffy JR, Strand EA, et al. APOE epsilon4 influences beta-amyloid deposition in primary progressive aphasia and speech apraxia. Alzheimers Dement. 2014 Nov; 10(6):630–6. [PubMed: 24985533]

48. van der Flier WM, Pijnenburg YA, Fox NC, Scheltens P. Early-onset versus late-onset Alzheimer's disease: the case of the missing APOE varepsilon4 allele. Lancet Neurol. 2011 Mar; 10(3):280–8. [PubMed: 21185234]

49. Mielke MM, Wiste HJ, Weigand SD, et al. Indicators of amyloid burden in a population-based study of cognitively normal elderly. Neurology. 2012 Oct 09; 79(15):1570–7. [PubMed: 22972644]

50. Barret O, Alagille D, Sanabria S, et al. Kinetic Modeling of the Tau PET Tracer (18)F-AV-1451 in Human Healthy Volunteers and Alzheimer Disease Subjects. J Nucl Med. 2017 Jul; 58(7):1124–31. [PubMed: 27908967]

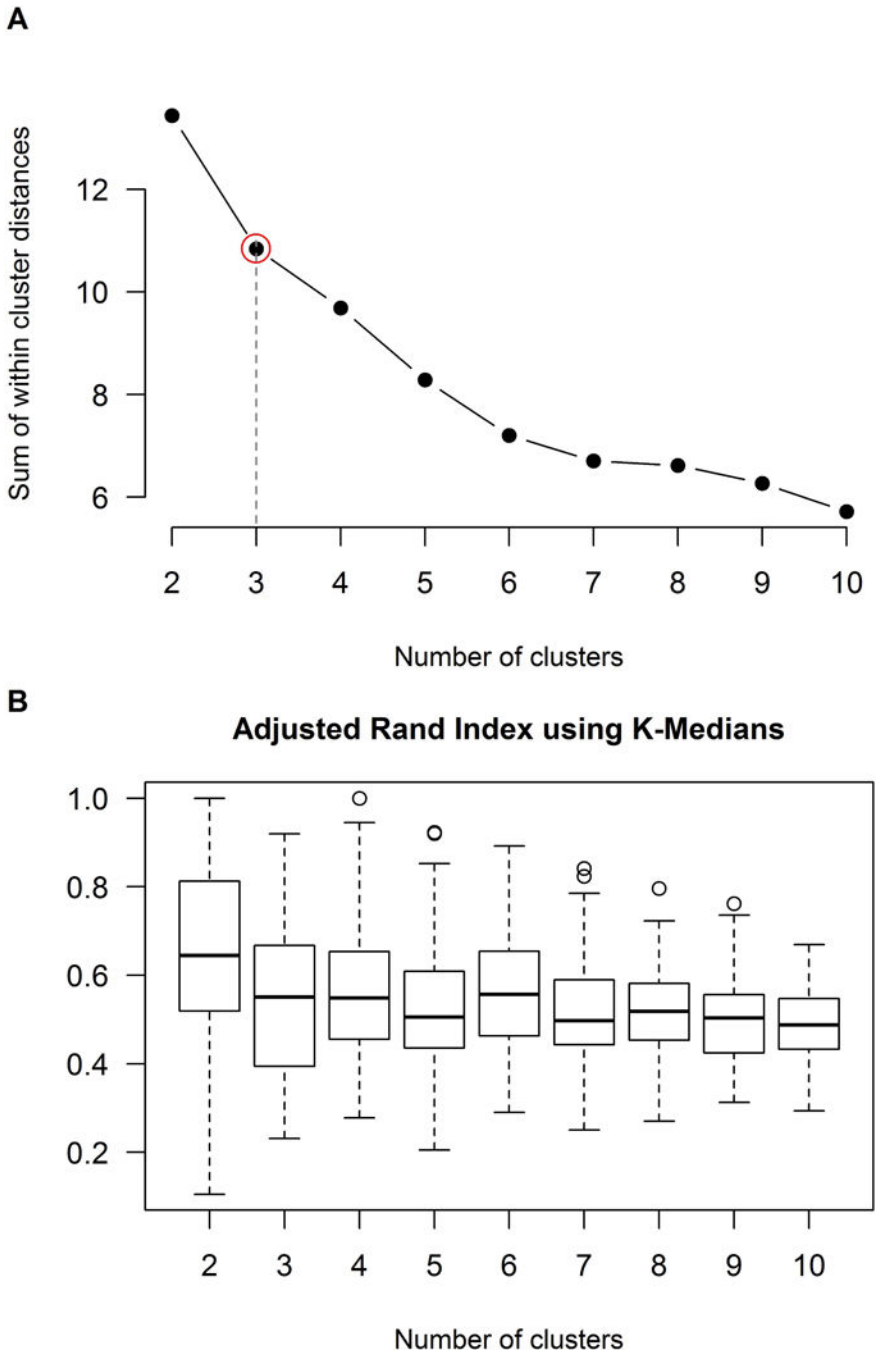

Figure 1. Analyses to determine appropriate number of clusters

Panel A shows a plot of sum of within cluster distances by number of cluster performed using the elbow method. This plot shows decreasing sum of within cluster distances with increasing cluster number. The aim is to try to minimize the sum of within-cluster distances, while choosing the smallest possible cluster size where adding one more cluster will offer little marginal improvements in the sum of within-cluster distances. Three clusters (i.e. the elbow, highlighted in red) showed a large reduction in sum of within cluster distances compared to just two clusters, with four clusters showing less additional reduction. Panel B

shows box plots summarizing the adjusted Rand index (ARI) by number of cluster. The ARI reflects concordance in clustering when performing bootstrapping resampling. The ARI analysis showed that cluster stability was similar for both three and four clusters. Given the results from both methods, three clusters was determined to be the optimum number of clusters for this dataset.

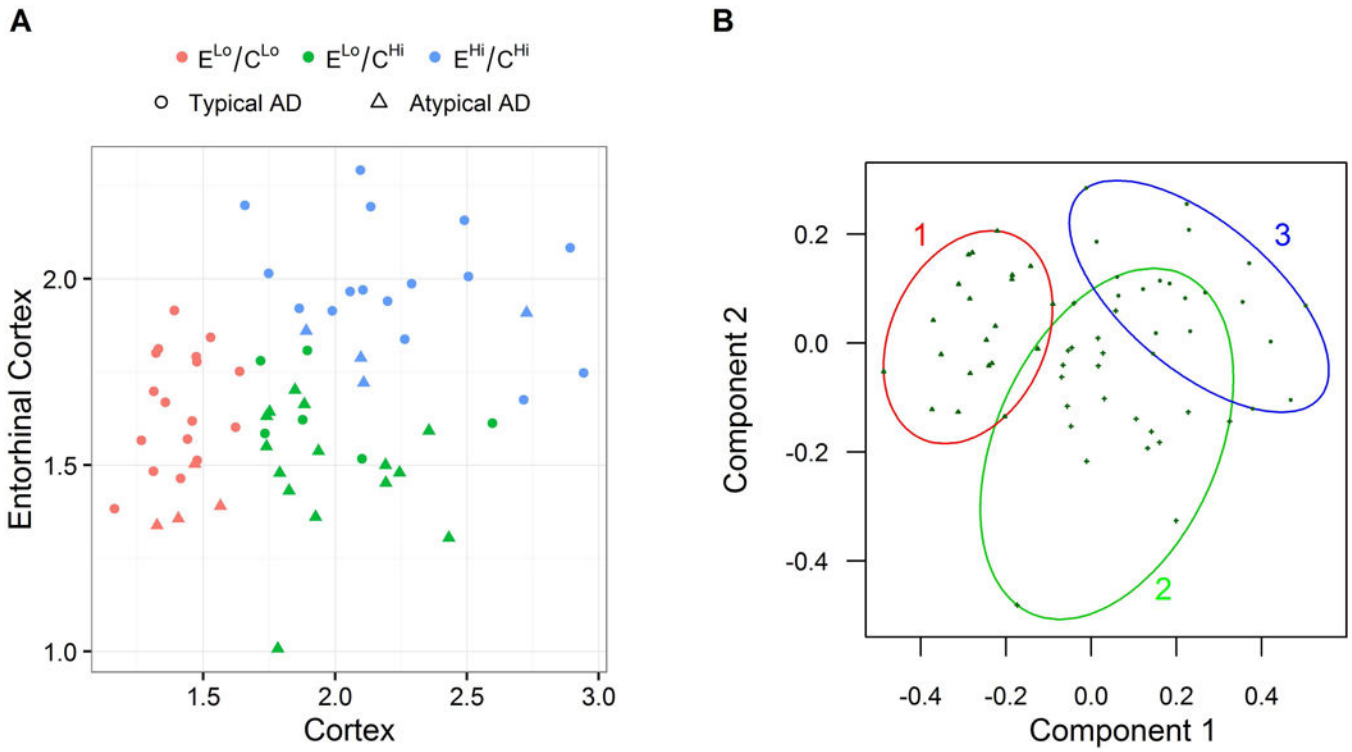

Figure 2. Results of the cluster analysis and principal component analysis

Panel A shows scatter-plot highlighting the K-medians clustering of patients into three clusters which we label E^{Lo}/C^{Lo} (red points), E^{Lo}/C^{Hi} (green points), and E^{Hi}/C^{Hi} (blue points). Clinical group is shown by symbol for each subject. Panel B demonstrates the separation of the three clusters via a scatter plot of the two principal components and overlaying ellipses drawn to include all points in each cluster.

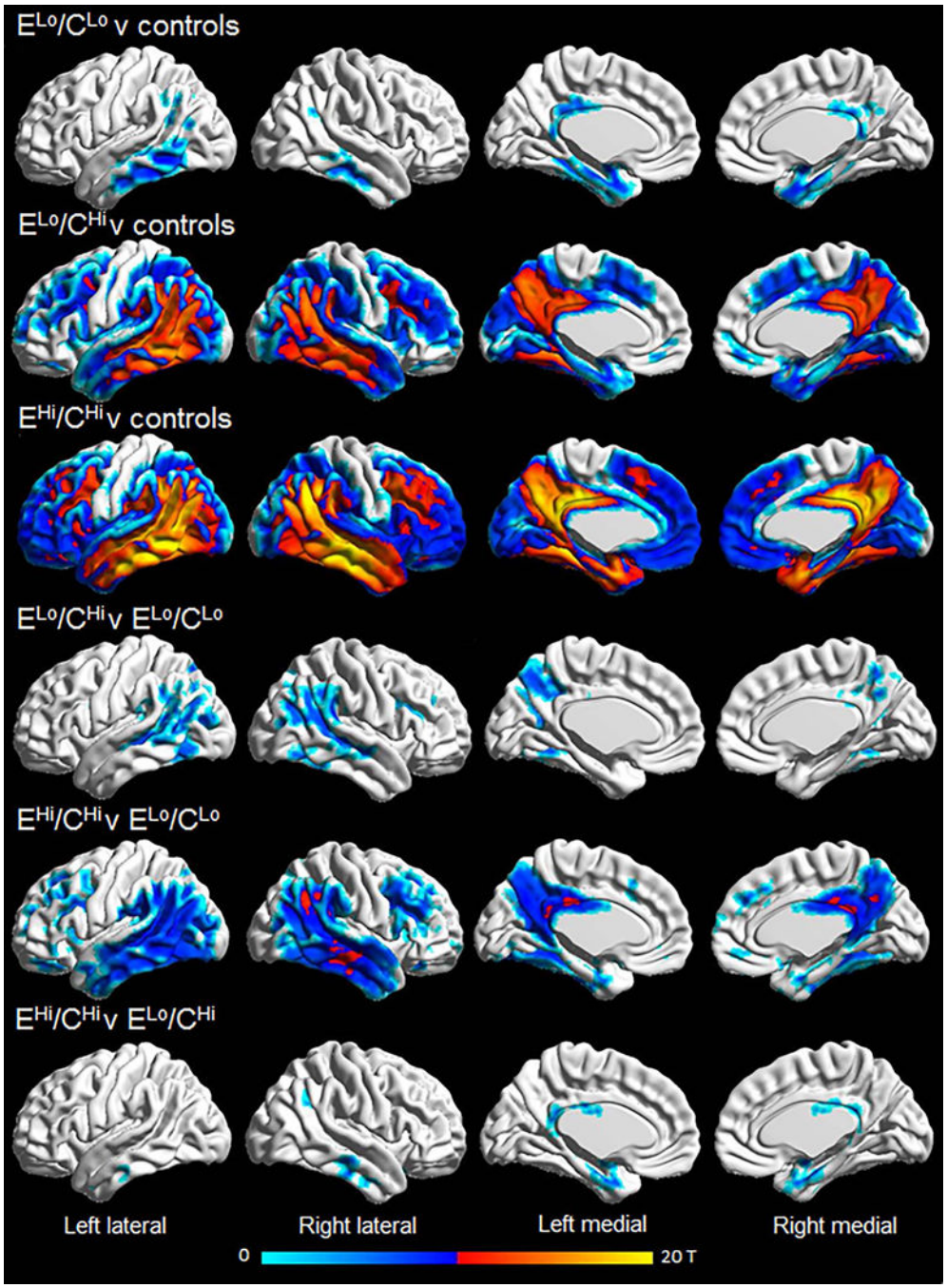

Figure 3. Voxel-level maps of tau-PET uptake in the three clusters compared to matched controls
Results are shown after correction for multiple comparisons using family wise error correction at $p<0.001$.

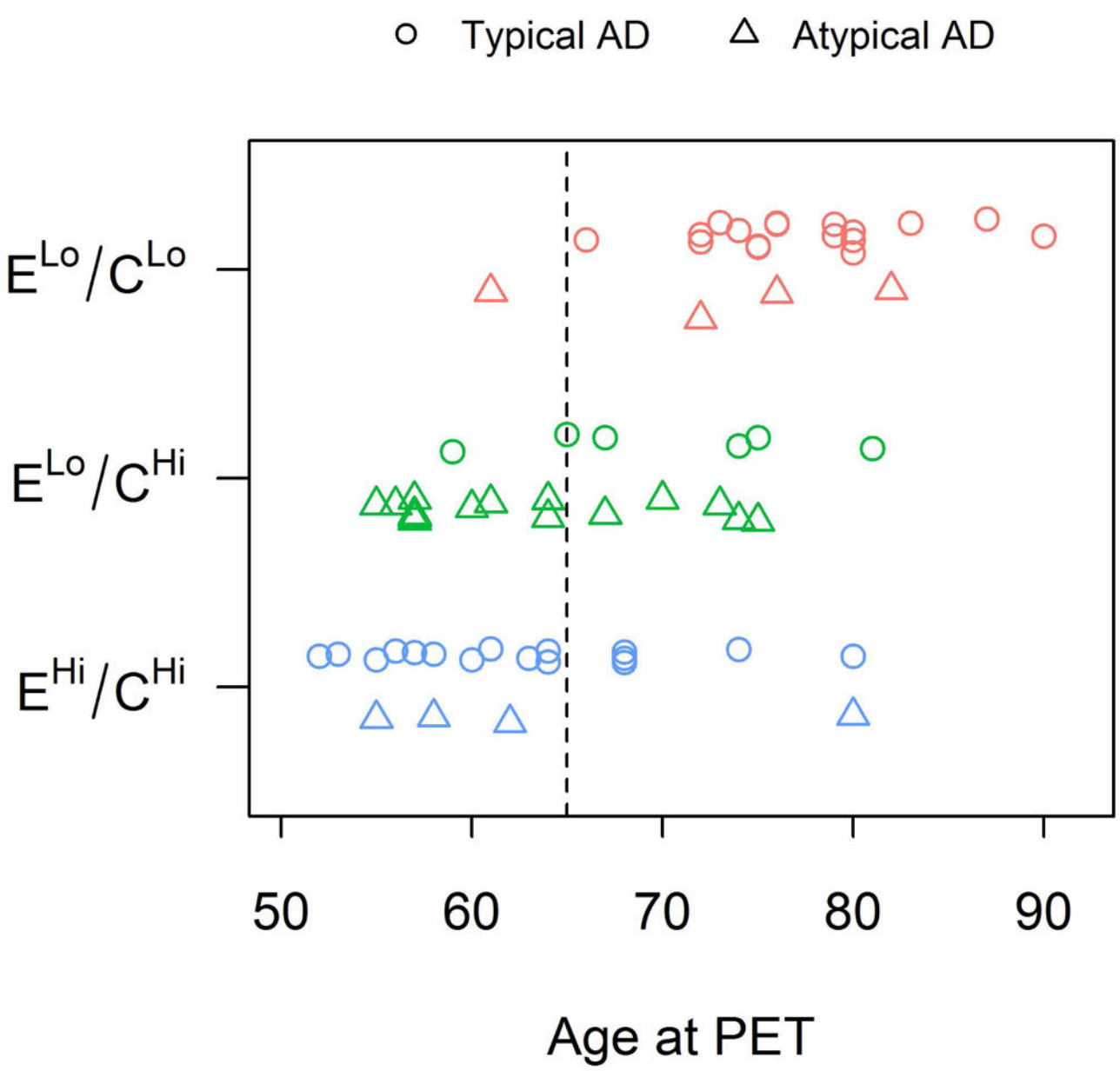

Figure 4. The distribution of age by cluster

The three K-Medians clusters are shown by color and clinical group is shown by symbol.

Table 1

Neuroimaging, demographic and clinical features by cluster

	E^{Lo}/C^{Lo} (n=21)	E^{Lo}/C^{Hi} (n=21)	E^{Hi}/C^{Hi} (n=20)	P
Neuroimaging features				
Entorhinal SUVRs	1.60 [1.48, 1.78]	1.55 [1.48, 1.63]	1.95 [1.85, 2.03]	<0.001 *
Cortical SUVRs	1.41 [1.32, 1.48]	1.88 [1.78, 2.19]	2.12 [2.04, 2.49]	<0.001 †
Entorhinal/Cortical SUVRs	1.13 [1.02, 1.23]	0.79 [0.68, 0.91]	0.87 [0.81, 1.00]	<0.001 ‡
Entorhinal gray matter volume (%TIV)	0.21 [0.16, 0.22]	0.23 [0.18, 0.25]	0.20 [0.19, 0.24]	0.29
Cortical gray matter volume (%TIV)	14.2 [12.6, 14.8]	13.3 [12.5, 14.1]	13.8 [12.8, 14.6]	0.36
PiB SUVRs	2.75 [2.43, 2.91]	2.45 [2.19, 2.64]	2.48 [2.23, 2.58]	0.02 ‡
Demographic features				
No. Female, n (%)	8 (38%)	12 (57%)	13 (65%)	0.22
APOE e4 Carrier, n (%)	16 (84%)	10 (48%)	14 (74%)	0.049 §
Age at Tau, yrs	76 [73, 80]	64 [57, 73]	62 [57, 68]	<0.001 ‡
Age at onset, yrs	70 [65, 74]	60 [55, 65]	55 [52, 62]	<0.001 ‡
Disease duration, yrs	5.58 [4.81, 9.09]	4.00 [2.92, 5.08]	4.05 [3.34, 6.86]	0.04 §
Clinical features				
AD type, n (%)				<0.001 ¶
Typical, n (%)	17 (81%)	6 (29%)	16 (80%)	
Atypical, n (%)	4 (19%)	15 (71%)	4 (20%)	
Atypical AD subtype, n (%)				0.37
Dysexecutive, n (%)	0 (0%)	5 (33%)	2 (50%)	
Logopenic progressive aphasia, n (%)	3 (75%)	3 (20%)	1 (25%)	
Posterior cortical atrophy, n (%)	1 (25%)	7 (47%)	1 (25%)	
CDR-SB	6.50 [4.25, 9.00]	3.00 [2.00, 4.00]	6.00 [2.00, 10.00]	0.16
Letter fluency (F)	8.00 [6.00, 17.00]	10.00 [7.00, 13.50]	10.00 [8.50, 96.00]	0.36
Animal fluency	9.00 [6.25, 15.50]	9.50 [7.75, 14.00]	14.00 [9.00, 96.00]	0.08 ‖
Trail Making Test A MOANS	9.00 [8.25, 10.00]	3.00 [2.00, 6.50]	9.00 [5.75, 11.00]	0.002 ¶
Trail Making Test B MOANS	7.00 [2.25, 8.00]	2.00 [2.00, 3.00]	7.00 [2.00, 9.00]	0.31
AVLT Delayed % Recall MOANS	6.00 [4.00, 6.00]	6.00 [4.00, 8.00]	2.00 [2.00, 4.50]	0.02 *
Rey-O MOANS	8.00 [7.00, 11.25]	2.00 [2.00, 5.25]	6.00 [3.00, 10.50]	0.01 §

APOE = apolipoprotein E; CDR-SB = Clinical Dementia Rating Scale Sum of Boxes; AVLT = Auditory Verbal Learning Test; Rey-O = Rey Osterrieth. MOANS = Mayo Older Adult Norms; TIV = total intracranial volume. MOANS scores are age corrected and constructed to have a mean of 10 and standard deviation of 3 among cognitively healthy subjects.

Data shown are n (%) or median [IQR]. P-values were assessed using Fisher's Exact and Kruskal Wallis Rank Sum tests.

* EHi/CHi is statistically different from ELo/CLo and ELo/CHi

† All groups are statistically different from each other

‡ ELo/CLo is statistically different from ELo/CHi and EHi/CHi

§ ELo/CLo is statistically different from ELo/CHi

¶ ELo/CHi is statistically different from ELo/CLo and EHi/CHi

// ELo/CHi is statistically different from EHi/CHi